Journal of Electroanalytical Chemistry 730 (2014) 34–40

Contents lists available at ScienceDirect

Journal of Electroanalytical Chemistry

journal homepage: www.elsevier.com/locate/jelechem

On the controlled electrochemical preparation of R_4N^+ graphite intercalation compounds and their host structural deformation effects

Adam J. Cooper [a], Matěj Velický [a], Ian A. Kinloch [b], Robert A.W. Dryfe [a,*]

[a] School of Chemistry, University of Manchester, Oxford Road, Manchester M13 9PL, UK
[b] School of Materials, University of Manchester, Oxford Road, Manchester M13 9PL, UK

ARTICLE INFO

Article history:
Received 15 May 2014
Received in revised form 18 July 2014
Accepted 21 July 2014
Available online 31 July 2014

Keywords:
Tetraalkylammonium
Intercalation
Graphite intercalation complex

ABSTRACT

We present electrochemical studies of tetraalkylammonium (R_4N^+) reduction chemistry at Highly Orientated Pyrolytic Graphite (HOPG) and glassy carbon (GC) electrodes. We show that by electrochemically controlled intercalation and formation of a graphite intercalation complex (GIC) into layered HOPG, the irreversible reduction of the tetraalkylammonium cation can be prevented and subsequent de-intercalation of the GIC *via* the use of potentiostatic control is achievable. R_4N^+ cations with varying alkyl chain lengths (methyl, ethyl and butyl) have been shown to exhibit excellent charge recovery effects during charge/discharge studies. Finally the effects of electrode expansion on the degree of recovered charge have been investigated and the observed effects of R_4N^+ intercalation on the graphite cathode have been probed by scanning electron microscopy (SEM) and X-ray diffraction (XRD).

1. Introduction

Ionic intercalation is a process by which insertion of an ionic species takes place into the lattice of a host structure. In the specific case of graphite, this can result in the formation of graphite intercalation complexes (GICs) [1–13] and in the case of tetraalkylammonium (R_4N^+) reduction at graphite cathodes, has been found to be accompanied by a significant irreversible volumetric expansion of the host graphite [14–16], irrespective of whether intercalation is electrochemical [17,18] or non-electrochemical [16,19]. Various chemical routes to R_4N^+ and alkali metal GIC syntheses have been presented [16,20–22] often taking place *via* cationic displacement reactions. Electrochemical procedures, on the other hand, are less common [23,24], despite the relative simplicity of cathodically charging a graphite electrode in the presence of a R_4N^+-containing electrolyte.

In aqueous media graphite cathodes are relatively inert, since the potentials associated with working in aqueous systems are restricted to the potential limits of water electrolysis [25], although the overpotential for hydrogen evolution is appreciable on graphite surfaces. In aprotic media however, where the solvent is cathodically sufficiently stable, graphite cathodes can be susceptible to attack by electron transfer between the electrolyte cations and the graphite cathode at sufficiently negative potentials [24].

R_4N^+ salts, with formula [$R_4N^+X^-$], where R represents the alkyl group and X represents the counterion, are commonly employed electrolytes in non-aqueous electrochemistry due to their low (negative) reduction potentials as well as their good solubility in aprotic media. As such the negative potential limit of many metallic electrodes has previously been assigned to the potential at which R_4N^+ degradation occurs [25]. In an oxygen free environment, it has been proposed by Dahm and Peters that R_4N^+ reduction at GC electrodes proceeds *via* an alkyl radical mechanism producing an alkyl carbanion, which is prone to reaction with a parent R_4N^+, thereby yielding various stable alkanes [26]. However, by performing the electrochemically controlled reduction at a layered graphite electrode (HOPG), the work herein shows that a reversible reduction process associated with intercalation takes place for R_4N^+ based electrolytes, and the resultant GIC can be de-intercalated and retrieved from the host structure using potentiostatic control.

The non-electrochemical preparation of tetrabutylammonium GICs has been reported by Sirisaksoontorn and co-workers [16], prepared *via* a cationic displacement reaction in which a sodium-ethylenediamine [$Na(en)_y^+$] complex within graphene galleries is rapidly displaced by tetrabutylammonium (TBA^+) cations. A stable GIC of formula $C_{44}TBA$ was formed, inducing an inter-plane expansion of 0.47 nm, smaller than the cationic diameter of TBA^+ (0.826 nm) due to the flexibility of the TBA^+ alkyl chains. Electrochemical production of R_4N^+ GICs presents a more controlled route, and allows for the de-intercalation of the GIC from the host

* Corresponding author.
E-mail address: robert.dryfe@manchester.ac.uk (R.A.W. Dryfe).

http://dx.doi.org/10.1016/j.jelechem.2014.07.025
1572-6657/

structure if desired [23,24,27], as well as offering control over the degree of intercalation and therefore the R_4N^+ GIC composition. Additionally, optimization of controlled electrochemical intercalation into graphite could offer a tunable production route towards monolayer, bi-layer and tri-layer graphene materials [28].

Besenhard and co-workers have presented Li^+ and tetramethylammonium (TMA^+) voltammetry at both graphite foil and platinum electrodes and give findings that are broadly consistent with those herein [23,24]. It has also been shown by Simonet and co-workers [25] that under dry solvent conditions, decomposition of R_4N^+ at platinum electrodes can be prevented and a platinum 'insertion' complex is achievable in a similar manner to GIC formation.

We expand on the previously reported work by showing that R_4N^+ GIC formation at layered HOPG electrodes can be reversible or irreversible depending on the magnitude of the applied charging load. Larger tetraalkylammonium cations (tetraethylammonium, TEA^+, and TBA^+) are also studied herein at HOPG electrodes, exhibiting similar charge recovery behaviour at surprisingly large charging potentials (*ca.* −3 V *vs.* $Ag/AgClO_4$), this phenomenon has not been previously reported to the best of our knowledge. This charge recovery cannot be performed at either GC or platinum electrodes, and the maximum degree of charge recovery is found to be related to the crystallographic diameter of the R_4N^+ species, as well as the initial thickness of the host graphite cathode. The reversible intercalation of lithium requires the irreversible formation of a protective solid-electrolyte interphase (SEI) layer at the electrode surface during initial charging (ESI, Fig. S1), whereas it has been shown by Sirisaksoontorn and Lerner [29] that during initial R_4N^+-GIC formation in solvents such as dimethyl sulfoxide, alkylation is required to passivate the graphite surface and stabilize subsequent GIC formation. Finally, the unique expansion of the graphite due to intercalation has been imaged using scanning electron microscopy revealing detailed segmented expansion rather than a uniform expansion.

2. Experimental

2.1. Materials

HOPG (SPI-1 grade, 10 × 10 × 1 mm) was obtained from SPI supplies (West Chester, PA, USA) and glassy carbon (GC, CHI 104 electrode, 3 mm diameter) from CH Instruments, Austin, USA. A $Ag^0/Ag^+ClO_4^-$ reference electrode was constructed in-house by placing a silver wire in a 3 mm diameter glass tube, sealed at one end with a Vycor®glass frit (Scientific and Medical Products Ltd., Cheadle, UK). The tube was filled with $AgClO_4$ (0.01 M) in 0.1 M of the chosen electrolyte in NMP, and is an example of a reference electrode of the first kind [30]; by which the potential of a metal is measured relative to its ion in solution. Finally the tube was sealed by heat shrinking.

The following chemicals were ordered from Sigma–Aldrich and used without further purification: N-Methyl-2-pyrrolidone (NMP, anhydrous, biotech. grade ⩾ 99.00%), lithium tetrafluoroborate ($LiBF_4$, 99.99%), tetramethylammonium perchlorate ($TMAClO_4$, 99.99%), tetramethylammonium tetrafluoroborate ($TMABF_4$, 99.99%), tetraethylammonium tetrafluoroborate ($TEABF_4$, 99.99%) and tetrabutylammonium tetrafluoroborate ($TBABF_4$, 99.99%). Independent Karl-Fischer titration revealed the anhydrous NMP to contain a residual water content of 0.0065%.

2.2. Methods

For reference, the potential of the ferrocene couple (Fe/Fe^+) in NMP was found to be *ca.* 0.43 V *vs.* $Ag/AgClO_4$. Tetraalkylammonium cations were chosen as the intercalating species. NMP was chosen as the electrochemical solvent due to its good solubility with respect to R_4N^+ containing electrolytes and graphene dispersing properties [31], as well as its large accessible reductive potential window [32].

R_4N^+-containing electrolyte (0.1 M) was dissolved in NMP (10 ml) in a glass cell in an oxygen free environment (argon saturated glove box, Pure lab, Innovative Technologies, USA). All potentials were controlled by a PGSTAT100 potentiostat (Autolab, Utrecht, The Netherlands) using Metrohm Autolab NOVA software. Unless otherwise stated, all electrochemical data was acquired in a pressurised glove box (+0.3 mbar *vs.* atmospheric pressure, $[O_2]$ = 0.1 ppm, $[H_2O]$ = 0.1 ppm). Voltammetry was scanned at 50 mV s^{-1} in all cases, unless otherwise stated. Finally, the potentials observed in the cyclic voltammetry (CV) were used to define those set in chronoamperometric mode to control the intercalation processes.

To ensure the maximum expulsion of residual water from the system, solutions were prepared in an argon saturated box where they remained throughout the duration of the work. Additionally, a fresh $Ag^0/Ag^+ClO_4^-$ reference electrode was prepared in the glove box and sealed. Unless otherwise stated, all potentials quoted herein are *vs.* $Ag/AgClO_4$. Between experiments, any apparatus requiring cleaning was removed from the glove box and washed with ethanol, after which it was reintroduced to the glove box and allowed to stand for a 30 min equilibrium period prior to reuse.

After electrochemical analysis, samples were analysed with scanning electron microscopy (SEM) and X-ray Diffraction (XRD). SEM images were obtained on a FEI Quanta 200 (E) SEM. XRD was performed on a Bruker D8 Discover X-ray diffractometer. Samples for SEM were placed vertically such that the edge planes were contacted to a carbon sticky pad and samples were gold sputtered in order to maximise conductivity of the delicately contacted HOPG.

3. Results

3.1. Tetraalkylammonium charge/discharge cycling

R_4N^+ cation intercalation was investigated using the NMP-based electrolyte. Zhang and co-workers have previously investigated [33] lithium intercalation using this system and found little SEI formation in NMP/$LiBF_4$, a finding attributed to the reductive inertness of this electrolyte system. Fig. 1 shows comparative CV current responses at both a GC electrode and a HOPG electrode

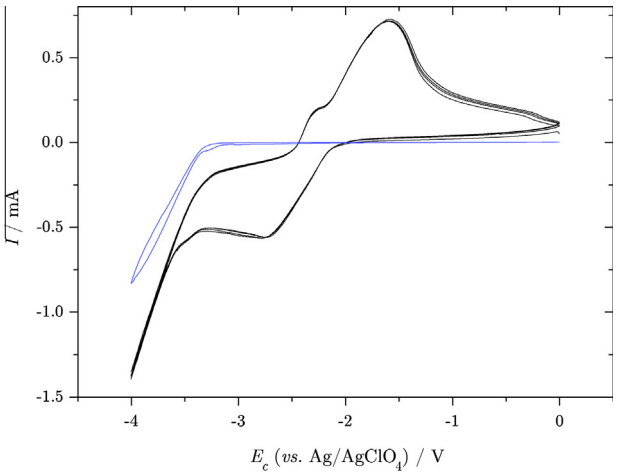

Fig. 1. Voltammetric response in 0.1 M $TEABF_4$ in NMP, scanned at 50 mV s^{-1} *vs.* $Ag/AgClO_4$, at a GC WE (blue line), and a HOPG WE (black line). (For interpretation of the references to colour in this figure legend, the reader is referred to the web version of this article.)

in a solution of $TEABF_4$ (0.1 M) in NMP. Only an increase in background current is observed when scanning at a GC electrode, which is attributed to the irreversible reduction of the electrolyte. When HOPG was employed as the working electrode, well-defined reduction and oxidation peaks appeared in the CV corresponding to the formation and subsequent collapse of a GIC, respectively. (Fig. 1, black scans). The voltammetry suggests that this GIC formation occurs at potentials more negative than *ca.* −2 V and is capable of being de-intercalated *via* the application of anodic potentials, shown by the large anodic current response at *ca.* −2 V on the reverse scan. The second reduction process at *ca.* −3.5 V is attributed to complete electrolyte and GIC reduction, *i.e.* the 'background current', and is sufficiently irreversible since there is no corresponding anodic peak on the reverse scan [34,35].

Charge/discharge was employed to probe the degree of generated charge associated with the respective intercalation and de-intercalation processes of R_4N^+ cations into HOPG. A 10 mg HOPG sample (*ca.* 0.1 mm thickness) was submerged by *ca.* 50%, exposing *ca.* 5 mg HOPG to the electrolyte solution. The 50% evaluation is an estimation conducted visually from outside the glove box. The degree of surface area change due to solvent evaporation was considered negligible, and was minimised with the use of a +0.3 mbar (*vs.* atmosphere) pressure. Initially, $TMAClO_4$ was investigated in parallel with the effect of intercalating potential. Charge/discharge cycling was performed in the same manner as lithium cycling, where the charging potential (E_c) was varied from −1.5 V through to −4 V, and discharge (E_d) was conducted at 0 V throughout. The resultant TMA^+ charge/discharge voltammetry is presented in Fig. 2, and the corresponding voltammetry for TEA^+ and TBA^+ is presented in ESI (Figs. S1 and S2).

It was found that extended R_4N^+ cycling had a permanent deformation effect upon the graphite cathode. During cycling, the HOPG electrode was observed to expand and did not collapse back to its original volume after the removal of applied potentials. This observed, irreversible expansion is in agreement with the work of Besenhard and Fritz in which they also observed irreversible graphitic deformation [24]. This expansion effect was not observed during comparable cycling with $LiBF_4$ (see supporting information, Figs. S3 and S4), even after 100 cycles, and is attributed to the crystallographic diameter of the R_4N^+ cations; 0.558 nm (TMA^+), 0.674 nm (TEA^+), and 0.826 nm (TBA^+) [36,37], being significantly larger than the interplanar spacing of HOPG (0.354 nm) [38] and the formation of the respective GICs. Indeed, the observed expansion was more dramatic for TEA^+ and TBA^+ cations than for TMA^+, where TMA^+ did not produce significant visible expansion within *ca.* 15 min, in contrast to the larger cations.

Somewhat surprisingly, in view of the subsequent structural changes of the electrode, it can be seen in Fig. 2(a) that the transients are relatively reproducible between cycles 2 and 5, indicating that the same process occurs each time once the system has been allowed to reach some equilibrium state (first cycle does appear to be different, attributed to initial double layer charging effects at the electrode, possibly related to surface oxide reduction).

It can be seen more clearly in Fig. 2(b) that when $E_c < -3$V the charging transients change shape and a sharp increase in the recorded current is observed approximately half way through the charge transient. The reproducibility of this feature is clear in all the cycles, which also increases in intensity with decreasing values of E_c. The kink in current is thought to be associated with the nucleation of a staged graphite intercalation compound [39]. The consequence of it is clearly observed in the larger than expected anodic peak current (*ca.* 13 mA) at $t = 0$ of the discharge transient and the developing shoulder on the de-intercalation transient. Both of these features are a result of the sudden increase in current observed in the charging transient and do not appear until

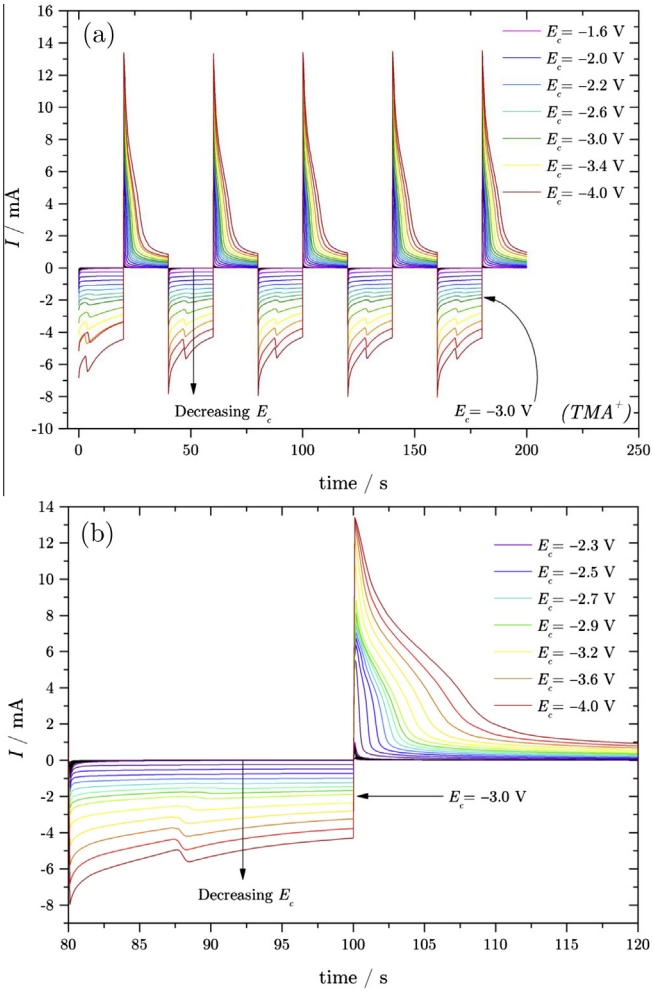

Fig. 2. TMA^+ charge/discharge plots showing (a) 5 cycles with decreasing E_c, and (b) enlarged third cycle.

$E_c < -3$V; the same threshold at which the cathodic current begins to steadily increase. These phenomena are likely to be linked. On the discharge transient, more so for more negative values of E_c, the rate of discharge is seen to vary over the total discharge with a gradient change visible, as opposed to a simple monotonic decay. This may be associated with the formation of the GIC on the charging process. The average charge efficiency ($\%_{ACE}$) of TMA^+ was calculated for the final four cycles and plotted against varying E_c as presented in Fig. 3.

Fig. 3 shows a selection of cycling efficiency trends derived from TMA^+ charge/discharge cycling data. Typical data sets obtained from the initial four cycles generally displayed variable charge ratios as large as *ca.* 15%; shown with the inclusion of error bars on each plot.

Fig. 3(a) shows a clear trend as E_c is decreased from −1.5 V to −4 V. In the initial stage, Stage I, where $-1.5\ \text{V} \geqslant E_c \geqslant -2\ \text{V}$, the $\%_{ACE}$ can be seen to decrease from *ca.* 100% to 75%. Here E_c values are within the potential region of little Faradaic activity, therefore the steady decrease can be attributed to small measurable changes in non-Faradaic current. To probe this, 25 cycles were recorded in an attempt to allow the system to reach some degree of stability, and data was extracted from the final four cycles. The resulting plot is presented as Fig. 3(b). It can be seen that the $\%_{ACE}$ can be recovered to nearly 100% by using data from longer periods of potentiostatic cycling. It is thought that this initial decrease in the charge recovery is a result of surface oxide groups present on the

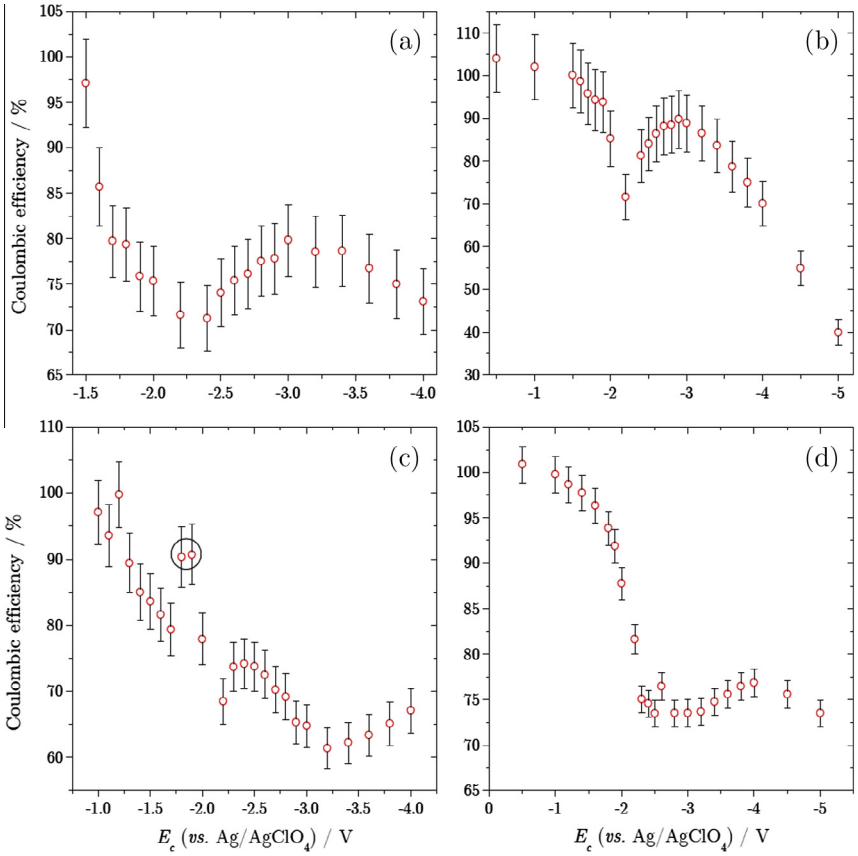

Fig. 3. Plots showing how TMA^+ charge/discharge efficiency is affected by decreasing E_c from values of −1 V to −5 V, (a) shows initial scans, (b) shows the effect of using data from extended cycling, (c) shows an example of 'anomalous' data (circled), and (d) shows the effect of using a thick (*ca.* 1 mm) HOPG sample.

graphite's edge and basal planes. This effect was also seen with lithium (see Supporting information, Figs. S3 and S4), and can explain why after prolonged cycling the system can behave in a more reversible fashion.

In Fig. 3(b) a sharp decrease in the $\%_{ACE}$ is observed at potentials around *ca.* −2 V. It should be noted that this phenomenon is not simply a result of reduced cycling times since repeated cycling (25 cycles) did not lead to complete recovery of cycling efficiency. The decrease in $\%_{ACE}$ could be attributed to partial intercalation without resulting associated electrode expansion, in which ions cannot fully de-intercalate from the host structure due to spatial restrictions. This hindrance to de-intercalation could be reflected in a decrease in total Q_d, since charge would remain at the electrode solution interface. An alternative explanation is the saturation of the electrode|solution interface with TMA^+, which is surface adsorbed and hence stabilized against associated decomposition. Blocking of the expanded electrode surface with these species would result in no stabilization of subsequently intercalated cations: resulting in complete irreversible reduction of these newly arriving species.

Interestingly, the $\%_{ACE}$ does not continue to decrease steadily and in Stage II, where $-2V \geqslant E_c \geqslant -3V$, the trend begins to increase. It was previously found that −2.4 V is the potential at which noticeable intercalation and electrolyte reduction occurs [40], and is also associated with the minimal potential required to result in observable electrode expansion of a HOPG electrode: this correlates with the gradient change of the plot.

During cycling in Stage I, occasional data points were noted with cycling efficiencies in excess of 90%, (Fig. 3(c), circled). These 'anomalous' points were only observed between E_c values of −1.5 V and −2 V and were observed most often with TMA^+. The sudden increase in efficiency is attributed to an increased de-intercalation flux during the discharge process. The excess number of ions is attributed to the previous charging cycles, in which some ions become trapped within the graphite pores. It is not until later stages of electrode expansion that these ions are allowed to de-intercalate freely, contributing positively to Q_d and observed as larger than expected efficiencies.

Finally, it was found that slightly different masses and thicknesses of initial HOPG samples affected the charges recovered. Fig. 3(d) shows the resulting $\%_{ACE}$ plot obtained when employing a relatively large mass of HOPG (13.6 mg) as the WE, approximately 10 times thicker than the samples generally used (1 mm *cf.* 0.1 mm). In Stage I of the plot, the trend is unchanged, but in Stage II charge is not recovered to the same extent as with thinner HOPG samples (75% *cf.* 90%). In addition, the $\%_{ACE}$ does not decrease at $E_c < -2$ V, but continues to produce cycling efficiencies greater than 70% even at E_c values as low as −5 V. Since Stage I is related to double layer charging, it follows that increasing the degree of accessible intercalation sites (thickness) has no effect on the double layer charging at the electrode. It is unclear at this stage why the cycling efficiency does not peak to near 100% efficiencies, as in the case of the *ca.* 0.1 mm study, given the introduction of more intercalation galleries in the *ca.* 1 mm study.

For graphical comparison, $\%_{ACE}$ plots for all R_4N^+ cations, and Li^+, have been presented on the same plot, as well as the result from testing at a GC (non-porous, non-expandable) electrode (Fig. 4). Error bars have not been included in this plot for the purpose of clarity, though there is approximately *ca.* 10% error included in the data. (The individual charge/discharge cycles from which Fig. 4 was constructed are given in the Supporting information: Figs. S1–S3, along with the $\%_{ACE}$ plots for TEA^+ and TBA^+, Figs. S5 and S6, respectively).

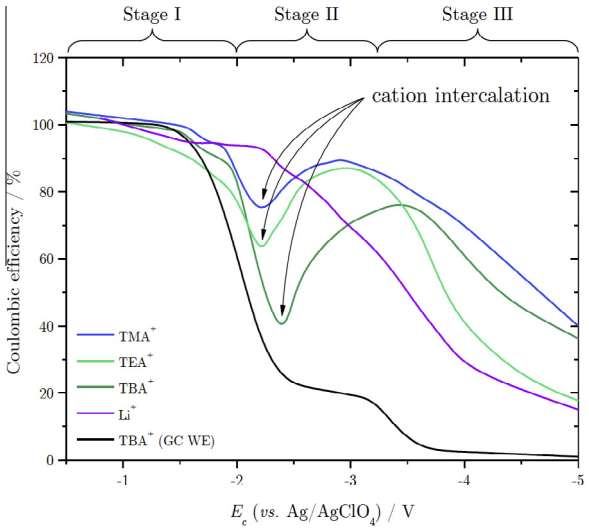

Fig. 4. ACE % plots obtained for (a) TMA^+, (b) TEA^+, (c) TBA^+ and (d) lithium and at a HOPG WE as well as (e) TBA^+ at a GC WE.

The most apparent aspect of Fig. 4 is the similarity of the trends shown by all three R_4N^+ cations. The R_4N^+ trends exhibit three clear stages in the cycling efficiency trends; the first stage is the relatively stable 100% cycling efficiency until E_c reaches *ca.* −2 V. Stage I is when $0V \geqslant E_c \geqslant -2V$ and is associated with two processes: (a) the electro-reduction of surface oxide groups present on the graphite cathode, which can eventually, with the use of prolonged charge/discharge electrochemical cleaning, be completely removed from the surface to allow near-100% cycling efficiencies, and (b) double layer charging of the electrode/solution interface, which resembles 100% cycling efficiency once surface oxides are removed from the electrode surface.

Stage II, when $-2\ V \geqslant E_c \geqslant -3\ V$, initially shows a sharp decrease in the cycling efficiency; indicating the onset of cation intercalation into the layered graphite structure. Intercalation has a stabilizing effect upon the R_4N^+ species, however at these relatively positive potentials, it is proposed that ion-trapping occurs where the degree of electrode deformation is such that removal of the intercalates cannot readily occur.

However, as Stage II progresses, a sudden recovery of $\%_{ACE}$ at *ca.* −2.2 V (for TBA^+ at *ca.* −2.4 V) begins. This feature is significant and has been attributed to permitted *reversible* intercalation, as a result of the onset of irreversible electrode expansion.

It is thought that electrode expansion has two implications; it allows cations trapped in the host structure from Stage I to de-intercalate freely back into the bulk electrolyte, contributing positively to Q_d. Secondly, and more significantly, it provides additional surface area at which the electrolyte double layer can form, allowing for additional Q_c storage at the electrode/electrolyte interface.

Eventually, in Stage III, the stabilization effects provided by the graphite expansion are unable to compete with the extreme cathodic conditions, and both the solvent and electrolyte are irreversibly reduced. This is reflected by the steady decrease in the cycling efficiency at potentials more negative than *ca.* −3 to −3.5 V.

These three stages have been labelled in Fig. 4, though it is important to note that although Stage I is relatively easy to define with the onset of intercalation and dramatic drop off of recoverable charge, there is a comparatively large degree of overlap between Stage II and Stage III due to the competing electrode expansion and electrolyte/solvent breakdown processes, as well as the elongation of potential observed with TBA^+.

Importantly, Fig. 4 shows that different maximum recoveries are achievable for the three R_4N^+ species, and this maximum recovery (between *ca.* −3 V and −3.5 V) is related to the increasing cation size. However it should be noted that there is a relatively large degree of error (between 5% and 10%) associated with the trends. The peak efficiency of the three cations is within a similar potential region, although that of TBA^+ is *ca.* 0.5 V more negative than that of TMA^+ and TEA^+. It should be noted that the potential at which charge recovery begins is *ca.* 0.25 V more negative for TBA^+ than for TMA^+ and TEA^+. This implies that TBA^+ intercalation requires slightly more negative potentials than the smaller cations, consistent with the greater diameter of TBA^+ requiring more energy to force the cation between the graphene galleries, indeed this is in agreement with voltammetry presented in previous work [40].

The decreasing peak efficiency with increasing crystallographic diameter suggests that the charge accommodated by the graphene galleries is the relevant factor, with more TMA^+ reversibly intercalated than TBA^+ species, simply as a result of spatial restrictions (as shown schematically in Fig. 5).

The amount of charge passed at the graphite electrode during the electrochemical intercalation of TEA^+, along with the mass of the graphite electrode involved, was used to estimate a TEA:C GIC composition ratio of 1:39, or $C_{39}TEA$, after a 10,000 s intercalation, although it is difficult to determine the exact mass (or equivalently, area) of graphite exposed to the solution in the present configuration. The intercalation stoichiometry is comparable to the $C_{44}TBA$ stoichiometry found by Sirisaksoontorn and co-workers [16]. Indeed, the total number of intercalated TEA^+ ions in this case may not necessarily remain stabilized in the form of a GIC and therefore the calculated ratio is more accurately described as an *initial* ratio; whether these GICs are stable or spontaneously de-intercalate remains to be established.

This effect could explain why the onset of complete TBA^+ reduction is seen at more negative potentials, since the stabilization energy from the neighbouring graphene sheets is delocalised over a greater area, offering effectively greater stabilization. The combination of improved TBA^+ stability (because of fewer intercalated species) along with a greater degree of TBA^+-trapping due to the comparatively lengthy alkyl groups, could contribute to the underlying reasons for the elongated cycling efficiency curve of TBA^+.

Finally, although the system is still competing with irreversible solvent breakdown at the most negative potentials, it is thought that the aforementioned cation stabilization effects help prevent solvent breakdown.

By contrast, the lithium and GC trends exhibit very little to no charge recovery mechanism, thus strengthening the hypothesis that electrode expansion is a result of intercalation into a layered structure, and has the direct consequence of stabilizing GICs: shown by the increase in cycling efficiency recovery. In this solvent

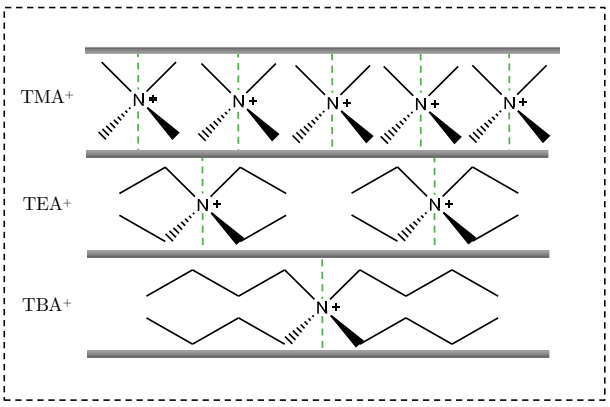

Fig. 5. Schematic, not to scale, highlighting the spatial restrictions incurred as a result of increasing cation size.

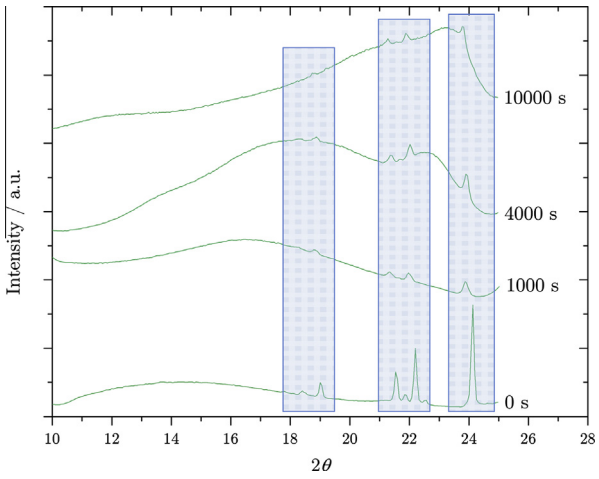

Fig. 6. Powder X-ray diffraction patterns for increasing TBA intercalation times into HOPG from 0 s (as prepared HOPG) to 10,000 s intercalation.

system, the lithium trend shows a steady decrease in the cycling efficiency with E_c, as a result of continuous non-recoverable SEI formation on timescales too short for sufficient coverage to allow for reversible lithium intercalation. Finally the TBA^+ trend at a GC electrode exhibits a slight plateau of the cycling efficiency, in the same potential region as the intercalation process is seen in the HOPG case. This indicates that a degree of charge recovery (or TBA^+ stabilization) is occurring, although no intercalation is possible at GC electrodes. This recovery occurs due to surface adsorption and subsequent stabilization; naturally the degree of stabilization from the adsorption mechanism is significantly less than that of the intercalation mechanism, since there is only one stabilization 'surface' provided by adsorption stabilization (Fig. S6(a)) in contrast to the 'two surfaces' provided by the graphene galleries during intercalation (Fig. S6(b)).

3.2. Electrode expansion

Intercalation of TBA^+ into HOPG using an applied potential of −2.4 V to the graphite cathode for successive periods of time (1000 s to 10 ks, at intervals of 1000 s) yielded the XRD patterns presented in Fig. 6. For the purpose of graphical comparison, the diffraction patterns have been scaled to one another and therefore their relative intensities are presented rather than their absolute intensities, similarly the prominent feature at $2\theta \approx 26°$, due to the (002) peak, has been removed from Fig. 6 to facilitate comparison of the weaker features. The 0 s pattern corresponds to the diffraction pattern of the as-prepared, non-intercalated HOPG sample, and shows the presence of crystallographic *d*-spacings in the range 2θ = *ca.* 18–25°. These diffractions are not prominent features, and are hidden well within the background signal, only becoming apparent after several hours of data acquisition.

The sub-lattice diffraction peaks are attributed to sub-lattice *d*-spacings created during the HOPG fabrication process, whereby gallery *d*-spacings are created between neighbouring graphite particulates as well as neighbouring graphene sheets. Theoretically these *d*-spacings might be expected to be greater than the 0.354 nm interplanar spacing of graphene sheets, since they are effectively artificial planes. It can be seen that these diffraction signals become less prominent with intercalation time, because the uniform expansion of the whole electrode begins to dominate, and the broad 'background' signal eventually masks the sub-lattice *d*-spacings (Fig. 6). Additionally, the peaks can be seen to shift slightly to smaller 2θ angles, indicating that their *d*-spacings are increasing.

These sub-lattice *d*-spacings clearly have an effect on the intercalation mechanism, since as the intercalation time increases the broad diffraction signal (*i.e.* the bulk exfoliation) begins to reside in the region of the pre-formed *d*-spacings. This is due to significant expansion of these artificial planes, causing overlap of their diffraction peaks and thereby adding to the general 'background'

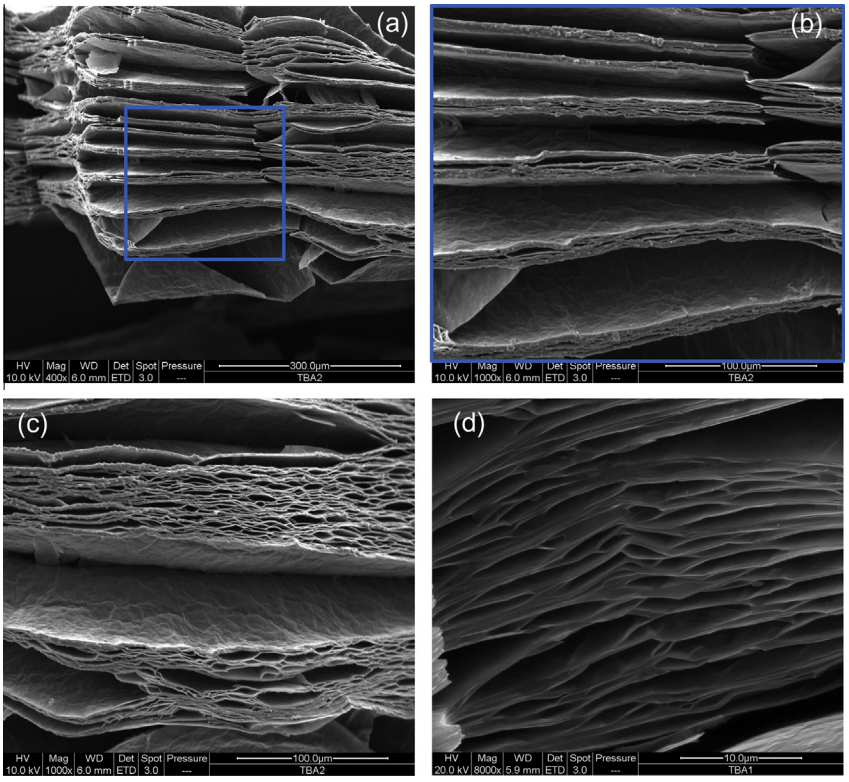

Fig. 7. SEM imaging of various segmented sections in an expanded portion of the same HOPG electrode, intercalated with TBA^+ for 10,000 s at −2.4 V.

expansion. It is believed that these pre-existing expanded galleries effectively act as energetically-favourable intercalation routes, by which intercalation preferentially occurs, since there are fewer steric restrictions associated with cations in these galleries than intercalating between the narrower 0.354 nm galleries. However as shown by the 'background signal' increase, intercalation is not completely restricted to these pre-existing galleries, and expansion is still allowed *via* the 0.354 nm galleries.

SEM of the same HOPG sample, analysed with XRD after 10,000 s of TBA^+ intercalation, shows (Fig. 7, see also ESI, Fig. S7) four areas of particular interest which were typical of the entire HOPG sample. All the images shown are relatively low magnifications (250–1000×) of the regular segmented expansion. The segmentation regularity is actually quite remarkable, where expansion occurs in groups, rather than uniformly throughout the structure. These 'large' groups are on the order of tens of microns thick and run for lengths as large as 1 mm. Closer inspection of these groups reveals that the 'large' micron groups are comprised of further subgroups.

The segmentation observed is consistent with the small angle diffraction planes observed in the XRD. Intercalation is thought to occur preferentially *via* these larger *d*-spacings since they effectively act as structural defects, allowing 'easier' intercalation, in which a smaller driving force is required, particularly for larger cations. To strengthen this argument, it was noted that electrode segmentation was not as prominent from TEA^+ and TMA^+ intercalation.

4. Conclusions

The electrochemical intercalation/reduction of tetraalkylammonium-containing electrolytes, and associated formation of GICs, has been studied using two types of carbon electrode. It has been found that potentiostatically controlled R_4N^+ intercalation results in the formation of GICs and allows for the controlled de-intercalation with the use of applied anodic potentials. TMA^+, TEA^+ and TBA^+ all show charge recovery ability during potentiostatic cycling, even at charging potentials as low as −3 V *vs.* $Ag/AgClO_4$. The observed charge recovery is possible because of the GIC stabilization induced by neighbouring graphene sheets and graphite expansion as shown by the poor charge recovery properties of TBA^+ reduction at a GC electrode. At sufficiently negative potentials, the stabilizing energy provided by the GIC conformation is overcome so irreversible reduction is unavoidable.

In agreement with Simonet and Lund [17], it has been shown here that the intercalation of TEA^+ and TBA^+ results in significant irreversible structural deformation of the graphite cathode. However despite the observed irreversible deformation, the charge cycling remains relatively stable, and R_4N^+ intercalation yields high (80%) charge recoveries at charging potentials as low as −3 V. This feat cannot be performed to the same extent at GC electrodes due to the non-porous nature of the electrode structure and limited degree of surface passivation: the maximum degree of charge recovery is found to be related to the crystallographic diameter of the R_4N^+ species, as well as the initial thickness of the host graphite cathode. The short-timescales associated with near-100% R_4N^+ charge recovery indicates the presence of some surface passivation to permit subsequent GIC stability, indicating that in systems containing R_4N^+ salts in NMP, the intercalation reversibility is greater than that of analogous systems containing lithium salts.

Microscopic segmentation was revealed through the use of SEM. The regularity of the observed segmentation was quite remarkable, and was also revealed during powder XRD studies in the form of sublattice planes in the as-prepared graphite samples at 2θ values in the region 10–25°. The expansion of the graphite electrodes was found to be non-uniform: it is thought that the electrodes expand preferentially *via* pre-existing galleries in the as-prepared HOPG lattice.

Conflict of interest

The authors declare no conflict of interest.

Acknowledgements

We thank the EPSRC – United Kingdom Grant funding (Grant references EP/I005145/1 and EP/K016954/1), and for a studentship for A.J.C.

Appendix A. Supplementary material

Supplementary data associated with this article can be found, in the online version, at http://dx.doi.org/10.1016/j.jelechem.2014.07.025.

References

[1] F. Beck, H. Krohn, E. Zimmer, Electrochim. Acta 31 (3) (1986) 371–376.
[2] B.J. Lee, Bull. Korean Chem. Soc. 23 (12) (2002) 1801–1805.
[3] T. Maluangnont, G.T. Bui, B.A. Huntington, M.M. Lerner, Chem. Mater. 23 (5) (2011) 1091–1095.
[4] R. Matsumoto, Recent advances in superconductive graphite intercalation compounds, in: C.B. Taylor (Ed.), Recent Advances in Superconductivity Research, Nova Science Publishers Inc., 2013, pp. 75–83.
[5] T. Nakajima, K. Nakane, M. Kawaguchi, N. Watanabe, Carbon 25 (5) (1987) 685–689.
[6] T. Nakajima, N. Watanabe, I. Kameda, M. Endo, Carbon 24 (3) (1986) 343–351.
[7] H. Shioyama, R. Fujii, Carbon 27 (6) (1989) 785–789.
[8] J.M. Skowroński, J. Urbaniak, Pol. J. Chem. 78 (9) (2004) 1339–1344.
[9] N.E. Sorokina, I.V. Nikol'skaya, S.G. Ionov, V.V. Avdeev, Russ. Chem. Bull. 54 (8) (2005) 1749–1767.
[10] K. Tasaki, J. Phys. Chem. C 118 (3) (2014) 1443–1450.
[11] M. Zhou, T. Tian, X. Li, et al., Int. J. Electrochem. Sci. 9 (2) (2014) 810–820.
[12] M.S. Zhou, C.J. Li, M. Xu, Y. Tao, Chinese J. Inorg. Chem. 22 (11) (2006) 2049–2054.
[13] M.S. Zhou, J.C. Xi, Adv. Mater. Res. 734–737 (2013) 2181–2186.
[14] Y. Geng, Q. Zheng, J.K. Kim, J. Nanosci. Nanotechnol. 11 (2) (2011) 1084–1091.
[15] T. Maluangnont, M.M. Lerner, K. Gotoh, Inorg. Chem. 50 (22) (2011) 11676–11682.
[16] W. Sirisaksoontorn, A.A. Adenuga, V.T. Remcho, M.M. Lerner, J. Am. Chem. Soc. 133 (32) (2011) 12436–12438.
[17] J. Simonet, H. Lund, J. Electroanal. Chem. Interfacial Electrochem. 75 (2) (1977) 719–730.
[18] G. Bernard, J. Simonet, J. Electroanal. Chem. Interfacial Electrochem. 96 (2) (1979) 249–253.
[19] W. Sirisaksoontorn, M.M. Lerner, Inorg. Chem. 52 (12) (2013) 7139–7144.
[20] Y. Mizutani, T. Abe, K. Ikeda, et al., Carbon 35 (1) (1997) 61–65.
[21] H. Shioyama, Y. Yamada, A. Ueda, T. Kobayashi, Carbon 43 (11) (2005) 2374–2378.
[22] A. Takenaka, T. Tsumura, M. Toyoda, Synth. Met. 160 (11–12) (2010) 1247–1251.
[23] J.O. Besenhard, Carbon 14 (2) (1976) 111–115.
[24] J.O. Besenhard, H.P. Fritz, J. Electroanal. Chem. Interfacial Electrochem. 53 (2) (1974) 329–333.
[25] J. Simonet, Y. Astier, C. Dano, J. Electroanal. Chem. 451 (1–2) (1998) 5–9.
[26] C.E. Dahm, D.G. Peters, J. Electroanal. Chem. 402 (1–2) (1996) 91–96.
[27] J.O. Besenhard, H. Möhwald, J.J. Nickl, Carbon 18 (6) (1980) 399–405.
[28] C.J. Shih, A. Vijayaraghavan, R. Krishnan, et al., Nat. Nanotechnol. 6 (7) (2011) 439–445.
[29] W. Sirisaksoontorn, M.M. Lerner, Carbon 69 (2014) 582–587.
[30] M. Velicky, K.Y. Tam, R.A.W. Dryfe, Anal. Method 4 (5) (2012) 1207–1211.
[31] Y. Hernandez, J.N. Coleman, Nat Nano 3 (9) (2008) 563–568.
[32] M.B.M. Breant, C. Buisson, M. Dupin et, J. Rebattu, Bulletin De La Societe Chimique De France 12 (810) (1968) 5065.
[33] S.S. Zhang, K. Xu, T.R. Jow, Electrochim. Acta 51 (8–9) (2006) 1636–1640.
[34] L.J. Hardwick, P.W. Ruch, M. Hahn, et al., J. Phys. Chem. Solids 69 (5–6) (2008) 1232–1237.
[35] P.W. Ruch, M. Hahn, F. Rosciano, et al., Electrochim. Acta 53 (3) (2007) 1074–1082.
[36] T. Osakai, K. Ebina, J. Phys. Chem. B 102 (29) (1998) 5691–5698.
[37] M.J. Stephenson, A.J. King, S.M. Holmes, R.A.W. Dryfe, J. Phys. Chem. B 109 (41) (2005) 19377–19384.
[38] K. Kinoshita, Carbon, Electrochemical and Physicochemical Properties, John Wiley & Sons, Inc., 1988.
[39] A. Funabiki, M. Inaba, T. Abe, Z. Ogumi, J. Electrochem. Soc. 146 (7) (1999) 2443–2448.
[40] A.J. Cooper, N.R. Wilson, I.A. Kinloch, R.A.W. Dryfe, Carbon 66 (2014) 340–350.